

Experimental evaluation and FDTD method for predicting electromagnetic fields in the near zone radiated by power converter systems

Mohammed LAOUR^{1,2,*}, Redouane TAHMI¹, Christian VOLLAIRE³

¹Research Laboratory in Electrical Engineering of ENP, National Polytechnic School of Algiers (ENP), Algiers, Algeria

²Development Unit of Solar Equipment (UDES)/EPST-EPST/Renewable Energy Development Center (CDER), Tipaza, Algeria

³Ampère Laboratory, University of Lyon, Central School of Lyon, Ecully, France

Received: 01.07.2015

Accepted/Published Online: 17.05.2016

Final Version: 10.04.2017

Abstract: This paper presents the study of conducted electromagnetic interference (EMI) currents flowing through the power cables of a DC-DC converter system and its correlation with the near field radiated from these cables. The radiated emission measurement contains a common mode (CM) and a differential mode (DM), and accurate separation of the radiated emissions of these two modes is necessary. The finite-difference time-domain (FDTD) method is used to predict the electromagnetic radiation caused by CM currents and DM currents. An experimental bench has been designed to allow access to the measurement of EMI disturbances at various sensitive places. The CM and DM voltages resulting from the experimental measurement are implemented in the FDTD algorithm as voltage sources of disturbances, these disturbance voltages causing the generation of CM and DM currents flowing through the cable. Finally, single and bifilar wire models for modeling the near field using the FDTD method are presented and the simulation results of the near field caused by both of the modes are evaluated and compared with the experimental ones. The main objective is to investigate the significance of the contribution of each of the current modes on the radiated emissions from the cable using the FDTD method, thus characterizing the level of cable radiation versus a specific standard. This allows showing that the radiation is often caused by the CM current along the cable and the largest level is located in the switching noise zone located within the frequency range from 1 MHz to 10 MHz.

Key words: Power electronics converters, finite-difference time-domain method, electromagnetic compatibility, electromagnetic interferences, common mode, differential mode

1. Introduction

Power switches are the excitation source at the origin of the radiation of power electronics converters because of the fast switching function of modern semiconductor devices such as MOSFETs and IGBTs. Their switching operation creates the appearance of very steep transition currents and voltages (high di/dt and dv/dt). The latter contain high frequency harmonics and cause differential mode (DM) emissions along the paths they travel through and components that they go across [1–3]. Moreover, potential variations are also created at the terminals of semiconductors and generate currents that flow through ground loops, which then can form significant radiation loops and which are not controlled in the system design stage. These currents are the cause of common mode (CM) radiation [4]. In addition, direct radiation from the converter is not the main

*Correspondence: mohammed.laour@g.enp.edu.dz

contribution of radiation often because of its small area, the conducted EMI currents flowing through the cables being the major problem to solve [5,6]. The separation of conducted and radiated emissions is necessary for the design of power electronic systems [7,8].

In this work, we present a prediction of the electromagnetic near field radiated by the power supply cable of a buck converter feeding a RL load, the system modeling constituting the starting point for this problem. The method chosen, the finite-difference time-domain (FDTD) method, is widely applied to solve different types of electromagnetic compatibility problems because of the need for wide frequency band results [9]. For this study, the FDTD method is based on specific measurement of CM and DM voltages generated by the buck converter and the evaluation of the equivalent CM and DM impedances of the system. This method requires only a voltage disturbance measurement in the time domain or predicted in the SPICE-based simulation environment (time domain), such as: Saber Software: Version W-2004.12, Saber®& CosmosScope™, which is a registered trademark of Synopsys [10]. The FDTD method is suitable for representing the thin wire in the model for simulation [11,12]; additionally, it is adjusted to show the integration of various linear lumped components into the model [13,14]. This simple and effective method allows estimating or directly calculating the electromagnetic field radiated by the cable in the time and frequency domain. It can show the electric and magnetic field mapping at different points of the circuit and only needs the source of the conducted disturbance to characterize the level of the electromagnetic field radiated in suitable conditions. The comparison with experimental results shows the validity of the model over a wide frequency range.

2. Experimental investigation

2.1. Schematic representation of the experimental bench

In order to verify the validity of our predictions, an experimental test bench was built as shown in Figures 1a and 1b. Measurements of conducted and radiated disturbances are realized in the anechoic chamber located in the Ampere Laboratory of Lyon, France. It was aimed to study the influence of unshielded cables on the near electromagnetic field level, so for radiated EMI measurements, the load, the control board, and the converter were confined as shown in Figure 1b. The containment was achieved by a metal case, which provided the function of shielding.

2.2. Schematic representation of the experimental setup and details

Figure 2 shows a schematic representation of the experimental setup and details. The disturbance voltages are measured through a line impedance stabilizing network (LISN) by using a high-voltage differential probe (LeCroy ADP305 with bandwidth: DC to 100 MHz) and an oscilloscope (LeCroy 66Zi HRO with a bandwidth: 400 MHz); these voltages are the cause of the disturbance currents flowing through the connection cable between the DC-DC converter and the LISN. These currents are considered as being the sources of the radiated EM field, whose near field distribution is predicted using the FDTD method, as will be explained in the following sections.

Figures 3a and 3b respectively show the time variation of CM and DM voltages resulting from the experimental measurement.

The measured CM voltage is obtained by the following formula:

$$V_{CM} = (V_{pLISN} + V_{nLISN})/2, \quad (1)$$

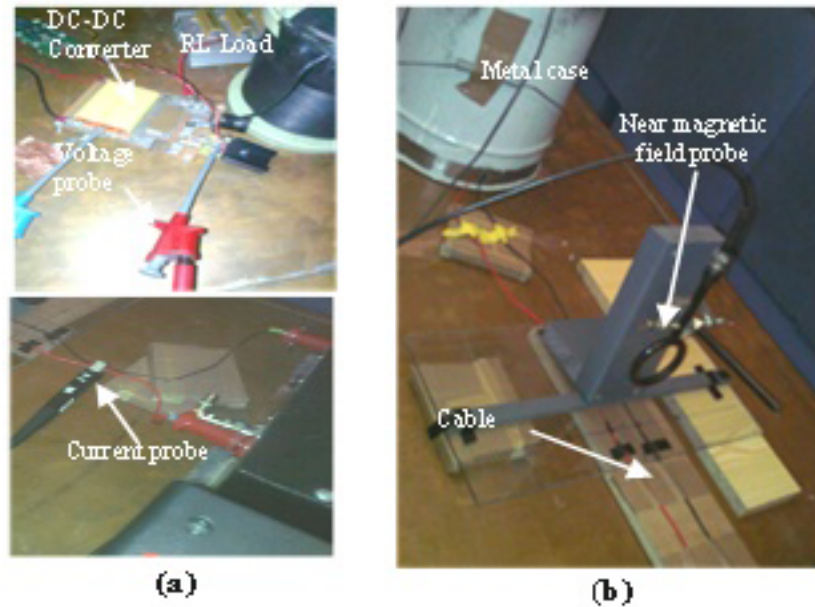


Figure 1. Schematic representation of the experimental bench: (a) measurement setup of conducted EMI, (b) measurement setup of radiated EMI.

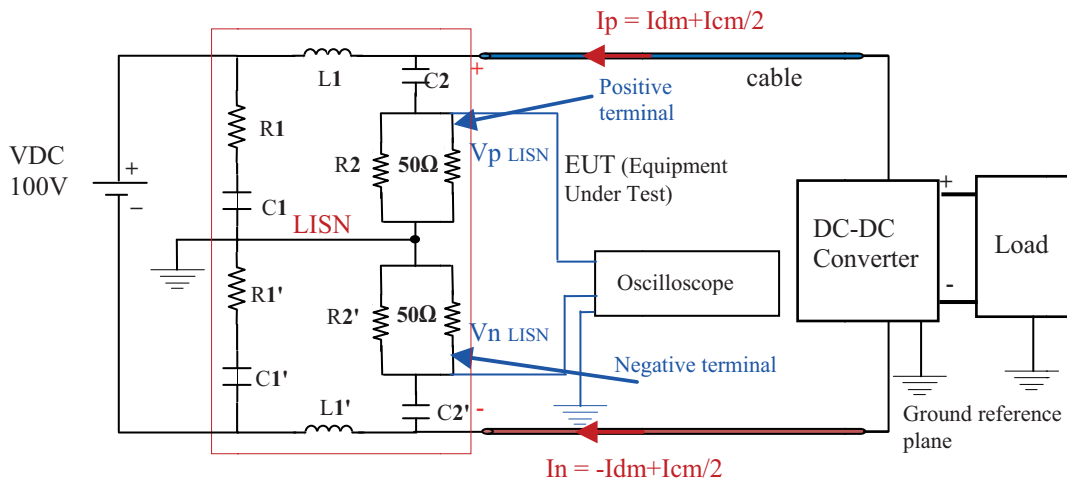


Figure 2. Schematic representation of the experimental setup and details.

and the measured DM voltage by:

$$VDM = (V_{pLISN} - V_{nLISN}), \quad (2)$$

where V_{pLISN} and V_{nLISN} are the voltages measured respectively at each measurement terminal of the LISN.

The measurement and operation conditions of this configuration are:

DC bus voltage: $VDC = 100$ V, Switching frequency: $f_s = 20$ KHz, Duty ratio of the MOSFET: $D = 0.5$.

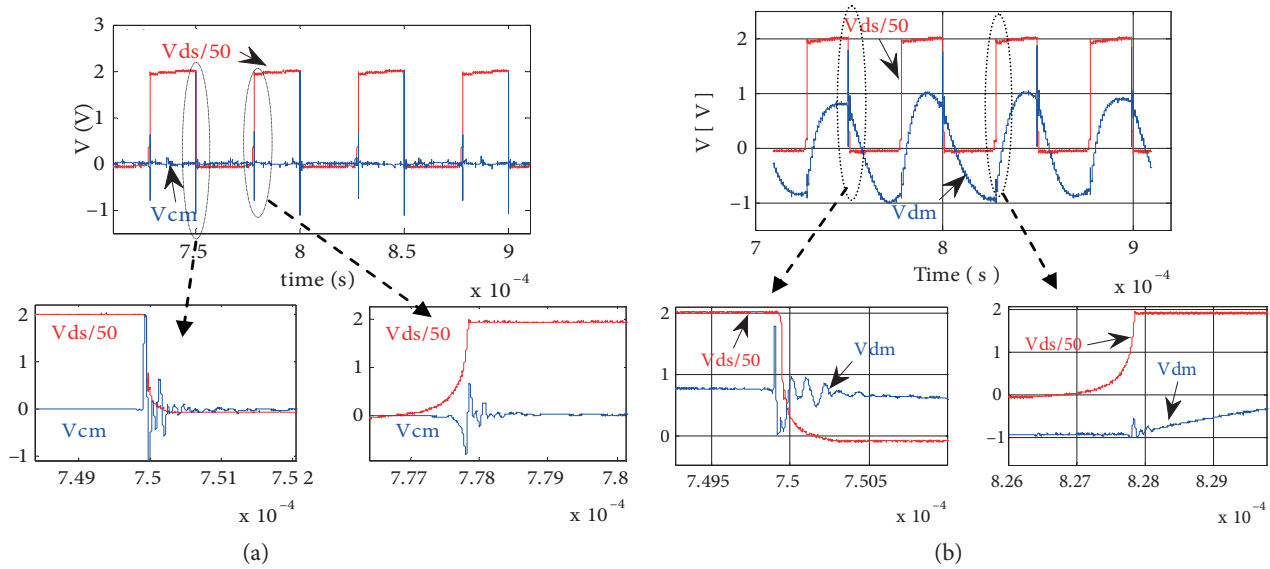


Figure 3. Time profile of drain-to-source MOSFET voltage V_{ds} (measured): (a) CM voltage disturbance measured through LISN, (b) DM voltage.

3. FDTD numerical model

3.1. Formulation

The FDTD method solves the time-dependent Maxwell equations in three-dimensional source-free space. The essential equations are the curl equations [15,16]:

$$\nabla \times E = -\mu \frac{\partial H}{\partial t}, \quad \nabla \times H = \varepsilon \frac{\partial E}{\partial t} + \sigma E, \quad (3)$$

$$\nabla \cdot E = \frac{\rho}{\varepsilon}, \quad \text{and} \quad \nabla \cdot H = 0, \quad (4)$$

where E is the electric field, H is the magnetic field, ρ is the charge density, ε is the permittivity, μ is the permeability, and σ is the conductivity.

The FDTD algorithm as proposed by Yee [17] in our calculation tools is a simple central-difference approximation to evaluate the space and time derivatives. Furthermore, in this algorithm, Berenger's perfect matched layer absorption boundary condition is adopted [18], the time step is constrained by the Courant–Friedrichs–Levy stability condition [15], and the numerical dispersion effects can be kept small by using a cell size Δs that is on the order of $\lambda/50$, where λ is the wavelength.

To obtain explicit update equations for the fields, the finite-difference approximations to the derivatives of Eqs. (3) and (4) need to be formulated. More details and a comprehensive overview may be found in [15,16].

3.2. Thin wire into the FDTD model

The simplest approach to include wires in the FDTD model is to model the thin wire as a perfect electric conductor (PEC). In this approach, all the corresponding tangential electric field components on the wire axis are permanently set to zero value.

To include the formality of the thin wire in the FDTD model, both the adjacent electric and magnetic fields of the wire are corrected according to its radius. The correction of the fields is carried out by equivalently

modifying the permittivity and permeability of the adjacent cells [9,19]. The electric field components around each thin wire are calculated using the modified permittivity $\varepsilon' = m \times \varepsilon$ and magnetic fields around each thin wire are calculated using the modified permeability $\mu' = m \times \mu$ where:

$$m \cong \frac{1.471}{\ln\left(\frac{\Delta s}{r}\right)}. \tag{5}$$

Here r is the wire radius.

3.3. Linear lumped elements in the FDTD model

Furthermore, to include the linear lumped elements in the FDTD model as shown in Figure 4, only the corresponding E components need to be modified to reflect the presence of an electric current density due to the lumped elements [12]. The following procedures are essentially based on the work of Picket-May [11].

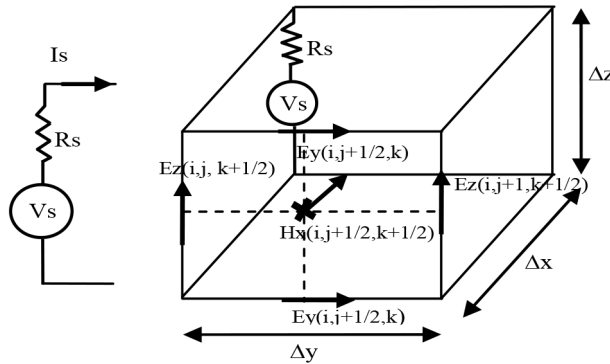


Figure 4. Update equations for Ezn (i, j, k) of voltage source and resistor.

The voltage Vn across the lumped element at time step n is defined by:

$$V^n = -E_z^n(i, j, k)\Delta S. \tag{6}$$

Therefore, the electric field component Ez for the resistive voltage source, which is considered as a source of disturbance, is given by the following equation according to [11].

$$\begin{aligned} E_z^{n+1}(i, j, k+1/2) &= k1.E_z^n(i, j, k+1/2) + k2.[H_y^{n+1/2}(i+1/2, j, k+1/2) - H_y^{n+1/2}(i-1/2, j, k+1/2)] \\ &+ k2.[H_x^{n+1/2}(i, j-1/2, k+1/2) - H_x^{n+1/2}(i, j+1/2, k+1/2)] - k3.\left[\frac{V_s^{n+1/2}}{\Delta z}\right] \end{aligned} \tag{7}$$

Here Vs is the source of disturbance (CM or DM voltage disturbance) and Rs is the internal impedance of the source.

$$k1 = \left(\frac{1 - \frac{\Delta t.\Delta z}{2R_s\varepsilon\Delta x.\Delta y}}{1 + \frac{\Delta t.\Delta z}{2R_s\varepsilon\Delta x.\Delta y}} \right), \quad k2 = \left(\frac{\frac{\Delta t.}{\varepsilon}}{1 + \frac{\Delta t.\Delta z}{2R_s\varepsilon\Delta x.\Delta y}} \right), \quad k3 = \left(\frac{\frac{\Delta t.\Delta z}{R_s\varepsilon\Delta x.\Delta y}}{1 + \frac{\Delta t.\Delta z}{2R_s\varepsilon\Delta x.\Delta y}} \right)$$

In the proposed model, we assume that $\Delta x = \Delta y = \Delta z = \Delta s$.

The electric field component Ez for resistive impedance is given by the same formulation of Ez for resistive voltage setting Vs = 0.

4. Validation of models

4.1. Common mode EMI equivalent circuit model

The equivalent FDTD model is illustrated in Figure 5. In this configuration, the unshielded cable consists of a single conductor for transmitting the power, and this is the metal structure (ground plane) that acts as a current return conductor. The source and the LISN are connected to the ground plane and only the CM current exists [4–6,20].

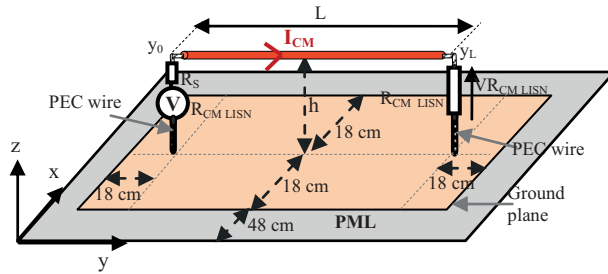


Figure 5. Equivalent FDTD model of CM current radiation for a cable.

The excitation source is the CM voltage evaluated at the terminals of the resistor of the LISN ($V_{R_{CM LISN}}$) with internal resistance R_s , which has the value of 0.1Ω and $R_{CM LISN} = 25 \Omega$. In the proposed model, the unshielded cable has a length L of 1.2 m and an equivalent radius $r = 1.5 \text{ mm}$, and it is situated at $h = 12 \text{ cm}$ over the ground plane. Cubic cells were employed with a spatial discretization of $\Delta s = \lambda_0/50$ and a size of time step of $\Delta t = \Delta s/2c_0$, where λ_0 is the minimum wavelength and c_0 is the free-space phase velocity.

Time-domain measurements were performed with the oscilloscope described previously in Section 2.2 with a bandwidth of 400 MHz and a maximum sampling frequency of 2 Gs/s ($\Delta t = 0.5 \text{ ns}$).

As illustrated in the experimental results, the measured CM voltage presents four periods of switching with time step size of $\Delta t = 0.5 \text{ ns}$. To simulate the developed model, the excitation source is taken at an interval of CM voltage that covers the transient switching phenomena of the converter (opening and closing switch: $50 \mu\text{s}$, which gives 100,000 as the number of time steps). To maintain the stability condition of the FDTD update process [15], data resampling is needed. With resampling of the excitation source in the time domain using MATLAB as shown in Figure 6a, $\Delta t = \Delta s/2.c_0 = 0.1 \text{ ns}$ is obtained, which gives $\Delta s = 6 \text{ cm}$ and 500,000 number of time steps for the FDTD simulation run. The maximum frequency calculated (fmax) of fast Fourier transform (FFT) can reach up to 100 MHz.

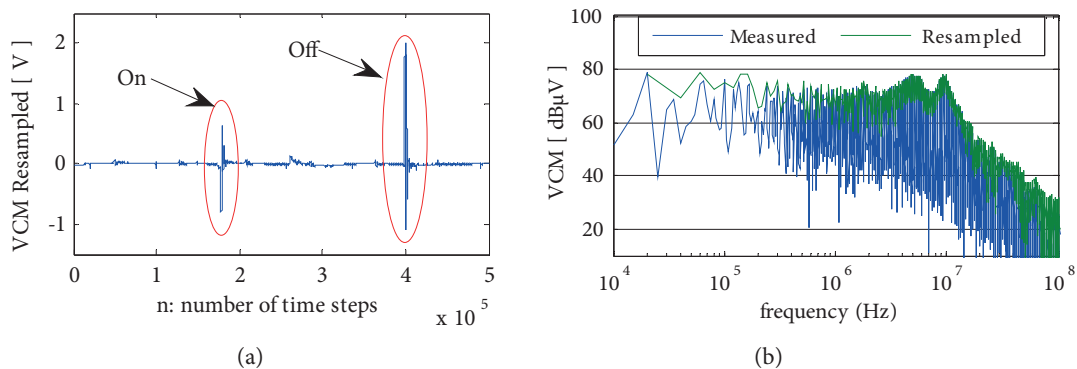


Figure 6. Resampling of CM excitation source voltage: (a) time domain, (b) frequency spectrum.

The frequency spectrum of the resampled excitation source is shown by the dashed curve in Figure 6b; this curve illustrates the envelope of CM voltage measured.

The CM current is the source of radiated disturbances. It can be calculated from the knowledge of the measured CM voltage and the CM impedance of the structure; the comparison result between CM calculated and measured respectively in the time and frequency domain is shown in Figures 7a and 7b.

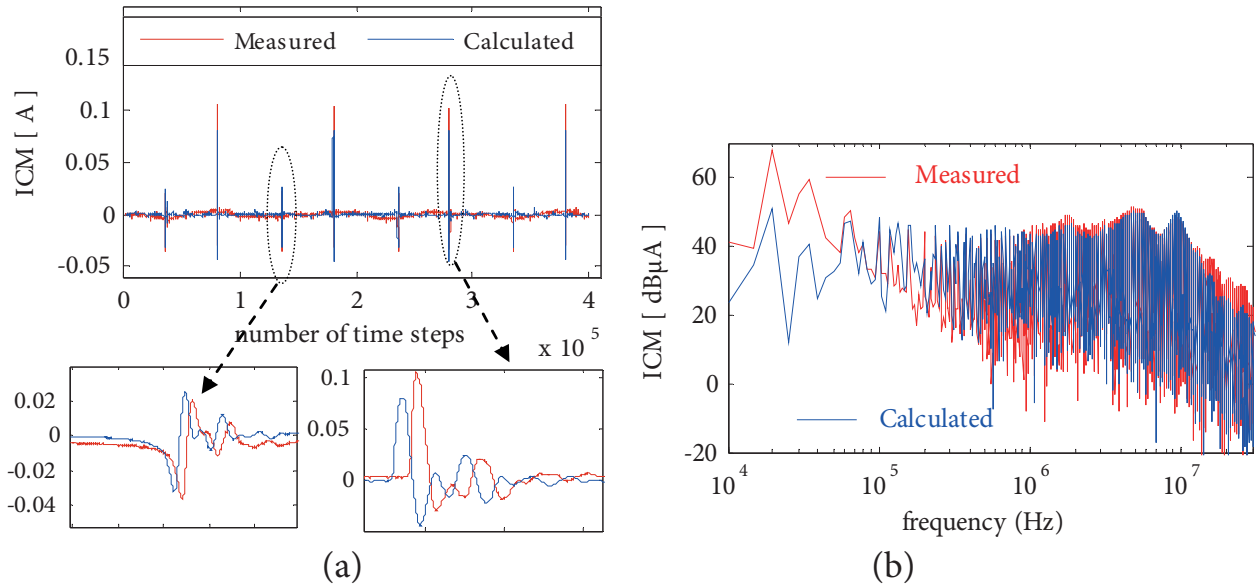


Figure 7. Comparison of CM current measured and that calculated from the ratio of the CM voltage measured and the CM impedance of the LISN: (a) time profile, (b) frequency spectrum.

The disturbance CM current has been measured using a current probe (Tectronics-TCPA 300, 100 MHz) with its amplifier (Tektronix-TCP A300-AC/DC) and an oscilloscope (LeCroy ADP305). This current is the main cause of the electromagnetic field radiation measured using the experimental bench.

Figure 7b presents the frequency spectrum comparison between the CM current measured by the current probe and the CM current flowing in the LISN that is calculated from the ratio of the CM voltage measured through the LISN and the CM impedance of the LISN. This result shows good agreement between the CM calculated and measured in the frequency range of 150 kHz to 30 MHz, where this frequency range corresponds to the stabilization of the impedance of the LISN according to the CISPR 16-2 standard [21]. In the frequency range of 10 kHz to 150 kHz, the difference in magnitudes among the results is due to the nonstabilization of the impedance of the LISN ($Z_{LISN} \neq 50 \Omega$).

4.2. Differential mode EMI equivalent circuit model

In order to simulate the proposed numerical model of the differential mode illustrated in Figure 8, the return of the current is carried by a conductor parallel to the outgoing conductor (the distance between the two conductors being $d = 12$ cm and it is situated at $h = 12$ cm over the ground plane). The converter is entirely isolated from the ground plane. In this configuration, only the DM current exists; the source of interference is the DM voltage supplied by the buck converter with internal resistance R_s , which is equal to 0.1Ω ; and the terminating impedance is the DM impedance of the LISN filter, which is equal to 100Ω .

For the simulation of the differential EMI model, the same procedure for determining the excitation source is adopted as in the case of the CM EMI model and its frequency spectrum is represented by the dashed curve in Figure 9.

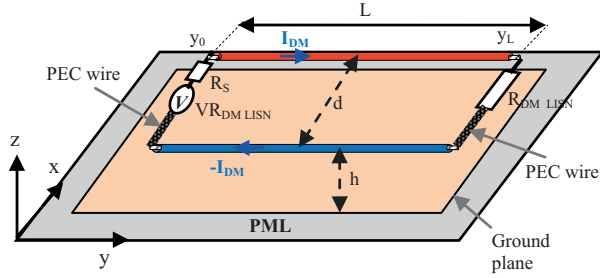


Figure 8. Equivalent FDTD model of DM current radiation for a cable.

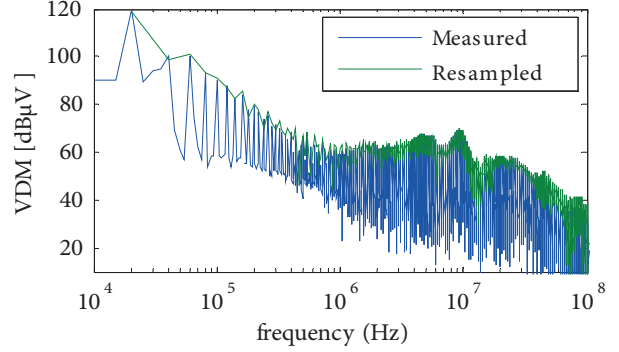


Figure 9. Frequency spectrum of resampling of DM excitation source voltage. Figure 10. Near magnetic field component H_x measured and simulated by using the FDTD method: (a) time profile, (b) frequency variation.

The radiated electric or magnetic fields due to each current mode can be summed in the time domain (with respect to the phases) to give the total radiated electric or magnetic fields (CM + DM).

The total radiated electric or magnetic fields can be calculated by:

$$E_{Total}(t) = E_{CM}(t) + E_{DM}(t), \quad (8)$$

$$H_{Total}(t) = H_{CM}(t) + H_{DM}(t). \quad (9)$$

4.3. Measurement and FDTD simulation results of magnetic field radiation

The near magnetic field has been measured by setting the loop sensor near the radiating element at 0.3 m above the cable at the midpoint of the conductors and connecting the probe to the oscilloscope in order to acquire the time-domain waveform of the voltage, which is induced by time-varying magnetic induction according to the Faraday law:

$$V_{in} = 2\pi \cdot f \cdot B \cdot A, \quad (10)$$

where B is magnetic induction, f is the frequency, and A is the section passed through by the magnetic flux.

This measurement is hidden by the poor signal/noise ratio due to the correction factor (Fa) of the H probe, which depends on frequency. This factor is introduced in the frequency spectrum analysis by using the FFT of the time representation of the measured magnetic fields, and the correction factor (Fa) is given by the manufacturer of the H probe.

Therefore, the measured magnetic field is obtained by the following formula:

$$H (dB\mu A/m) = Fa (dB) + Vin (dB\mu V). \quad (11)$$

Figures 10a and 10b respectively show the time and frequency variation of the near magnetic field H_x measured and that due to CM and DM simulated by the FDTD method at 0.3 m above the conductors.

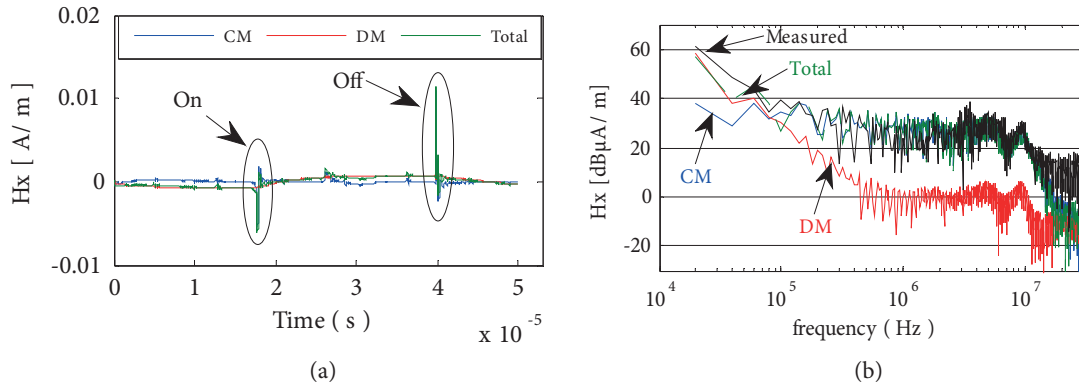


Figure 10. Near magnetic field component H_x measured and simulated by using the FDTD method: (a) time profile, (b) frequency variation.

The comparison results generally show that good agreement is observed between the measurement and those obtained by employing the FDTD model. This finding is clear in the frequency range of 150 kHz to 10 MHz, while in the frequency range of 10 MHz to 30 MHz, a difference of a few dB between the results may result from the inaccurate calculation of the CM and DM impedances, where resonance peaks exist in this frequency range.

From these results, it can be seen that the dominant emission mode regarding the magnetic field is the CM radiation. These results confirm the relevance of the developed FDTD simulation tool.

Figure 11 shows the strength distribution of the maximum magnetic field level H_x component that is due to CM current resulting from FDTD simulation during opening of the switch at $n = 180$ with $t = n \times \Delta t$, $\Delta t = 31.25$ ps, $L = j \times \Delta s$ and $h = k \times \Delta s$, $\Delta s = 1.87$ cm, and $i_0 = 10$.

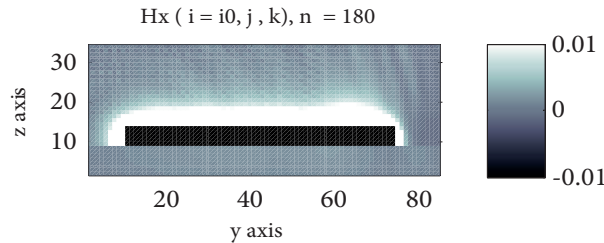


Figure 11. Magnetic field strength H_x (A/m) component distribution due to CM current during opening of the switch, resulting from FDTD simulation.

Here n and Δt are the index and size of the time step; Δs is the spatial increment in the x , y , and z directions; and i , j , and k denote the indices of spatial increments respectively in the x , y , and z directions.

4.4. Electric field evaluation

As the proposed simulation tool is validated for the magnetic field, it can now be used for evaluating the E components of the near fields radiated by the cable in real conditions. In this study, despite the inability to experimentally validate the evaluation of the electric field, only the E components of the near field simulation by FDTD method will be presented and the requirements of the DO 160E standard [21] will be indicated. The simulation conditions are always the same as those in the previous case.

Figures 12a and 12b respectively show the time and frequency variation of the near electric field E_z component due to CM and DM current derived by employing the FDTD method at 1 m above the conductors.

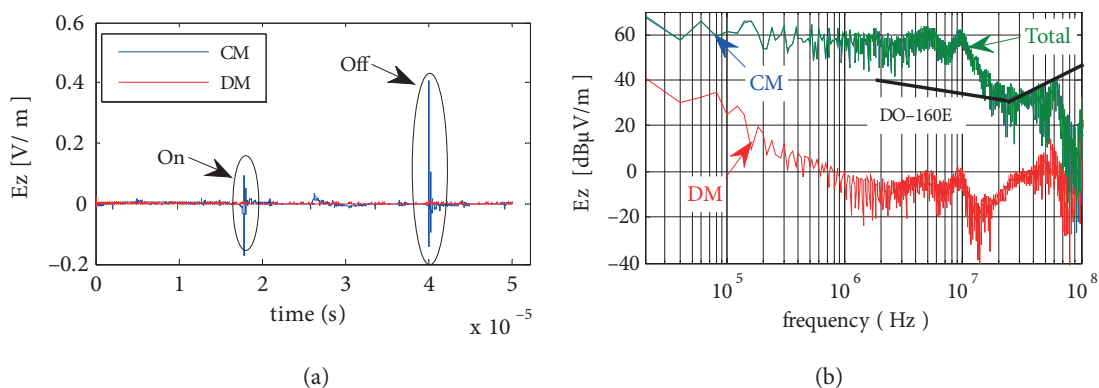


Figure 12. Near electric field E_z component resulting from FDTD simulation: (a) time profile, (b) frequency variation.

From Figure 12b, it can be noted that the electric field level does not meet the template set by the DO-160E standard [22,23], drawn in black in the figure. It is also noted that the largest level of electric field that exceeds the template of the standard is located in the switching noise zone located within the frequency range from 1 MHz to 10 MHz, which requires an effective filtering to be put in place to limit this disturbance. Above 10 MHz, the noise level drops due to the fall of the intrinsic level of the disturbance source.

It can also be seen that beyond 15 MHz and up to 100 MHz, the electric field radiated in DM increases with frequency by 30 dB. The radiation in CM decreases by 30 dB in this frequency range. Generally, CM radiation is considered as being the main source of radiation of power electronics converters and the corresponding power supply cables.

Figure 13 shows the intensity distribution of the maximum electric field level obtained by FDTD simulation during opening of the switch at number of time steps n indicated in Figure 13. Here $t = n \times \Delta t$, $\Delta t = 31.25$ ps, $L = j \times \Delta s$, and $h = k \times \Delta s$, where $\Delta s = 1.87$ cm, $i_0 = 10$, and $kp = 10 + h$.

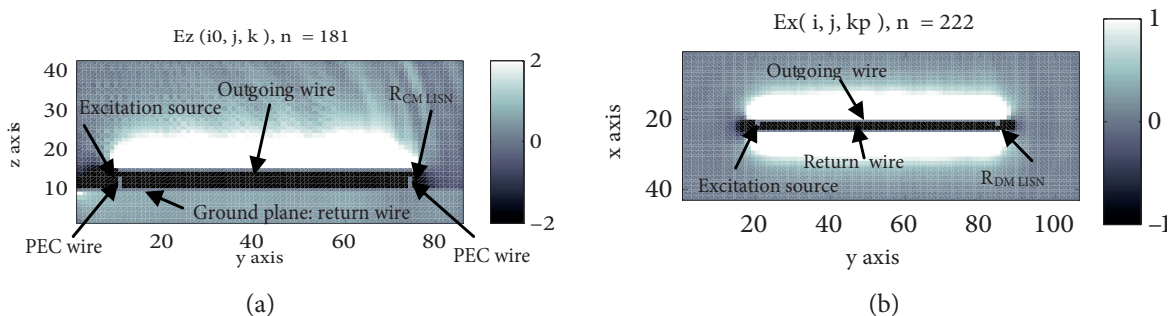


Figure 13. Electric field strength during opening of the switch: (a) E_z (V/m) component due to CM current, (b) E_x (V/m) component due to DM current.

As a result, it is important to understand that the FDTD method is costly in terms of computation time, although as computing resources continue to improve the trends in power electronics are going to lead to the design of power converters with high switching frequencies in order to reduce the total size and weight of the equipment [24]. This method will be less costly in terms of computation time; thus, it is the most convenient tool to study the radiated emissions of power electronics converters.

In order to explain this finding, we consider the Table, which shows the relationship between the switching frequency (f_s) and the number of time steps (n) for the FDTD simulation run of our models studied previously with the same simulation conditions.

Table. Relationship between switching frequency and run-time of our FDTD models.

Switching frequency (fs)	Number of time steps (n)
20 kHz	500,000
150 kHz	66,667
300 kHz	33,333
1 MHz	10,000
3 MHz	3333

5. Conclusion

In this paper, the concept of the near field radiated by CM and DM currents using the FDTD method has been presented. A three-dimensional FDTD model was developed and employed to study the electromagnetic near field radiated by the power supply cable of the DC-DC converter and due to each of the current modes. The EMI models of each current mode were simulated using MATLAB in the time domain. The simulation was performed after resampling of the excitation source in the time domain to cover a wide frequency range. Using this simulation tool, the emission source can be evaluated and the electromagnetic field computed. Furthermore, the significance of each current mode on the radiated emissions from the cables has been investigated.

The efficiency of the proposed numerical model under adequately specified conditions of use has been experimentally confirmed and a comparison between the measured and computed magnetic field has been presented. Experimental studies were carried out by the establishment of the experimental device by exploiting the characteristics of an anechoic EM chamber. The developed numerical model requires only the measurement of voltage disturbance in the time domain or its simulation using the computer tools that have been developed to model and simulate the EMI generated by power electronics converters in the time domain, while this measurement or simulation does not need the use of an anechoic EM chamber or very expensive instrumentations.

References

- [1] Paul CR. Introduction to Electromagnetic Compatibility. 2nd ed. New York, NY, USA: Wiley, 2006.
- [2] Paul CR. A comparison of the contributions of common-mode and differential-mode currents in radiated emissions. *IEEE T Electromagn C* 1989; 31: 189-193.
- [3] Chen H, Qian Z. Modeling and characterization of parasitic inductive coupling effects on differential-mode EMI performance of a boost converter. *IEEE T Electromagn C* 2011; 53: 1072-1080.
- [4] Kaires RG. The correlation between common mode currents and radiated emissions. In: *IEEE 2000 International Symposium on Electromagnetic Compatibility*; 21–25 August 2000; Washington, DC, USA. New York, NY, USA: IEEE. pp. 141-146.
- [5] Meng J, Ma W, Zhang L. Determination of noise source and impedance for conducted EMI prediction of power converters by lumped circuit models. In: *IEEE 2004 Power Electronics Specialists Conference*; 20–25 June 2004; Aachen, Germany. New York, NY, USA: IEEE. pp. 3028-3033.
- [6] Bishnoi H, Baisden AC, Mattavelli P, Boroyevich D. Analysis of EMI terminal modeling of switched power converters. *IEEE T Power Electr* 2012; 27: 3924-3933.
- [7] Stahl J, Kuebrich D, Duerbaum T. Characterisation of an effective EMI noise separation including a standard LISN. In: *IEEE 2010 International Symposium on Electromagnetic Theory*; 16–19 August 2010; Berlin, Germany. New York, NY, USA: IEEE. pp. 13-16.
- [8] Caponet MC, Profumo F. Devices for the separation of the common and differential mode noise: design and realization. In: *IEEE 2002 Applied Power Electronics Conference and Exposition*; 10–14 March 2002; Dallas, TX, USA. New York, NY, USA: IEEE. pp. 100-105.

- [9] Çakır G, Çakır M, Sevgi L. Electromagnetic radiation from multilayer printed circuit boards: a 3D FDTD-based virtual emission predictor. *Turk J Elec Eng & Comp Sci* 2009; 17: 315-328.
- [10] Rondon E, Morel F, Vollaire C, Schanen JL. Modeling of a buck converter with a SiC JFET to predict EMC conducted emissions. *IEEE T Power Electr* 2014; 29: 2246-2260.
- [11] Baba Y, Nagaoka N, Ametani A. Modeling of thin wires in a lossy medium for FDTD simulations. *IEEE T Electromagn C* 2005; 47: 54-61.
- [12] Mäkinen RM, Juntunen JS, Kivikoski MA. An improved thin-wire model for FDTD. *IEEE T Microw Theory* 2002; 50: 1245-1255.
- [13] Piket-May M, Taflove A, Baron J. FDTD modeling of digital signal propagation in 3-D circuits with passive and active lumped loads. *IEEE T Microw Theory* 1994; 42: 1514-1523.
- [14] Chu, QX, Hu XJ, Chan KT. Models of small microwave devices in FDTD simulation. *IEICE T Electron* 2003; E86: 120-125.
- [15] Taflove A, Hagness S. *Computational Electrodynamics: The Finite-difference Time-domain Method*. 3rd ed. Boston, MA, USA: Artech House, 2005.
- [16] Taflove A, Brodwin ME. Numerical solution of steady-state electromagnetic scattering problems using the time-dependent Maxwell's equations. *IEEE T Microw Theory* 1975; 23: 623-630.
- [17] Yee KS. Numerical solution of initial boundary value problems involving Maxwell's equations in isotropic media. *IEEE T Antenn Propag* 1969; 14: 302-307.
- [18] Berenger JP. A perfectly matched layer for the absorption of electromagnetic waves. *J Comput Phys* 1994; 114: 185-200.
- [19] Berenger JP. A multiwire formalism for the FDTD method. *IEEE T Electromagn C* 2000; 42: 257-264.
- [20] Ala G, Di Piazza MC, Tine G, Viola F, Vitale G. Evaluation of radiated EMI in 42-V vehicle electrical systems by FDTD simulation. *IEEE T Veh Technol* 2007; 56: 1477-1484.
- [21] International Electrotechnical Commission. *Specification for Radio Disturbance and Immunity Measuring Apparatus and Methods - Part 2-1: Methods of Measurement of Disturbances and Immunity - Conducted Disturbance Measurements*. CISPR 16-2-1; Rev. 1.1. Geneva, Switzerland: IEC, 2005.
- [22] RTCA Inc. *Environmental Conditions and Test Procedures for Airborne Equipment*. RTCA/DO-160F. Washington, DC, USA: RTCA Inc., 2007.
- [23] Costa F, Gautier C, Revol B, Genoulaz J, Démoulin B. Modeling of the near-field electromagnetic radiation of power cables in automobiles or aeronautics. *IEEE T Power Electr* 2013; 28: 4580-4593.
- [24] Majid A, Saleem J, Bertilsson K. EMI filter design for high frequency power converters. In: *IEEE 2012 International Conference on Environment and Electrical Engineering*; 18–25 May 2012; Venice, Italy. New York, NY, USA: IEEE. pp. 586-589.